Remote sensing of NO_2 emission from the central urban area of Shanghai (China) using the mobile DOAS technique

Shanshan Wang,[1,2] Bin Zhou,[1] Zhuoru Wang,[1] Suna Yang,[1] Nan Hao,[2] Pieter Valks,[2] Thomas Trautmann,[2] and Limin Chen[1]

Received 6 October 2011; revised 28 April 2012; accepted 29 May 2012; published 7 July 2012.

[1] The mobile DOAS technique was used to quantify the NO_x vehicle emission of the central urban area, enclosed by the Inner Ring Viaduct Road (IRVR), of Shanghai, China. Three field measurement campaigns were performed during the pre-EXPO period in October 2009, the EXPO opening ceremony, and the closing ceremony period in 2010. The spatial and temporal distributions of NO_2 Vertical Column Densities were derived, and the effects of traffic and wind conditions were studied. The averaged NO_2 emissions rates from the IRVR area were determined to be 2.1 $\pm$ 0.9 ton/h, 2.8 $\pm$ 1.4 ton/h and 2.7 $\pm$ 1.4 ton/h for these three campaigns. The annual vehicle NO_x emissions for the central urban area were estimated to be (2.3 $\pm$ 1.0) $\times$ 10^4 ton in 2009 and (3.0 $\pm$ 1.5) $\times$ 10^4 ton in 2010, and those for the whole city were (13.4 $\pm$ 5.9) $\times$ 10^4 ton in 2009 and (17.6 $\pm$ 8.4) $\times$ 10^4 ton in 2010, by considering a typical NO/NO_2 ratio, NO_x lifetime, as well as the traffic emission share of central urban area with respect to the entire city. The vehicle NO_x emissions quantified by mobile DOAS were found to exhibit an increasing trend in the central urban area of Shanghai, by 1.6 times and 2.1 times from 2006 to 2009 and 2010. Due to wind field variations, unknown NO_x chemical transformation, and uncertainties in AMFs, the systematic derivation of the final NO_x emission rates obtained was about 55% for averaged several consecutive days.

Citation: Wang, S., B. Zhou, Z. Wang, S. Yang, N. Hao, P. Valks, T. Trautmann, and L. Chen (2012), Remote sensing of NO_2 emission from the central urban area of Shanghai (China) using the mobile DOAS technique, *J. Geophys. Res.*, *117*, D13305, doi:10.1029/2011JD016983.

1. Introduction

[2] Shanghai, located on the alluvial plain of the Yangtze River Delta (YRD), is the economic center of China, and one of the mega-cities in the world. Its residential population at the end of 2009 was more than 19 million, with an area of 6340 km^2 covering 17 districts and one county. Due to the rapid economic growth, the vehicle population has increased with an average rate over 10% per year during the last decade, and there are currently more than 2.85 million vehicles registered in Shanghai [*Shanghai Municipal Statistics Bureau*, 2001–2010]. As a result, vehicle emission has become a major source of urban air pollution in Shanghai [e.g., *Chan and Yao*, 2008; *Wang et al.*, 2010]. In particular, the total NO_x emission in the central urban area surrounded by the Inner Ring Viaduct Road (IRVR) is largely contributed by vehicle emission [*Wang et al.*, 2008; *Fu*, 2009]. Therefore, the quantification of vehicle emissions is fundamental to complementing and updating the emission inventory.

[3] The World Exposition (EXPO) 2010 was held on both banks of the Huangpu River in Shanghai, from 1 May to 31 October 2010. With the theme of "Better City - Better Life," the air quality in Shanghai has attracted more and more attention [*United Nations Environment Programme* (*UNEP*), 2009]. To improve and maintain the air quality, the municipal government implemented a series of strategies to control and reduce the vehicle emissions before and during the EXPO, including employing the National Fourth Phase Emission Standards (equivalent to the Euro 4 standards) from November 2009 onwards, accelerating to phase out obsolete polluting vehicles before the EXPO started, and introducing several access limitations [*UNEP*, 2009]. Since 2009, heavy-duty vehicles which failed to meet the Euro 2 standards for exhaust emissions have been banned from entering the IRVR area. Similarly, all vehicles not compliant with Euro 1 standards have been prohibited to enter the middle ring viaduct road from August 2009 onwards [*UNEP*, 2009]. During the EXPO, only vehicles with the EXPO pass were permitted to enter the EXPO Park surrounding areas.

[4] The Differential Optical Absorption Spectroscopy (DOAS) remote sensing technique, based on molecular UV-VIS light absorption, has been proven to be an important

[1]Department of Environmental Science and Engineering, Fudan University, Shanghai, China.
[2]Remote Sensing Technology Institute, German Aerospace Center, Wessling, Germany.

Corresponding author: B. Zhou, Department of Environmental Science and Engineering, Fudan University, Shanghai 200433, China. (binzhou@fudan.edu.cn)

0148-0227/12/2011JD016983

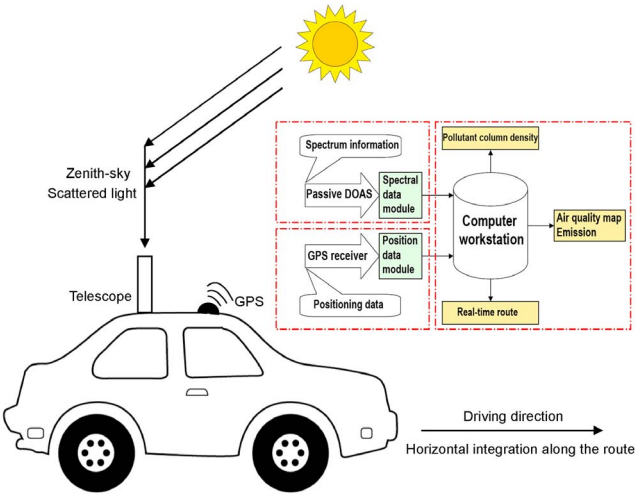

Figure 1. Schematic framework of the mobile DOAS system used in Shanghai.

tool for air pollutant field measurements [*Platt and Stutz*, 2008]. Employing zenith scattered sunlight, passive DOAS is capable of measuring tropospheric and stratospheric species such as NO_2 [e.g., *Petritoli et al.*, 2002], O_3, BrO and OClO [e.g., *Fraser et al.*, 2009]. Passive DOAS can be carried out on various platforms including ground-based [e.g., *Chen et al.*, 2009] or mobile stations [e.g., *Johansson et al.*, 2008, 2009], and airborne [e.g., *Giovanelli et al.*, 2006] or satellite-borne facilities [e.g., *Petritoli et al.*, 2004; *Martin*, 2008]. With the ability to measure many gases simultaneously in open atmosphere and the portability on a moving platform, the mobile DOAS technique has been employed for measuring NO_2 and SO_2 plumes emitted from a power plant [e.g., *McGonigle et al.*, 2004], SO_2, BrO in volcanic plumes [e.g., *Bobrowski and Platt*, 2007], as well as emissions from industrial areas [e.g., *Rivera et al.*, 2009, 2010] and from the entire cities [e.g., *Johansson et al.*, 2008; *Ibrahim et al.*, 2010].

[5] In order to investigate NO_x vehicle emissions from the central urban area of Shanghai, we applied the mobile passive DOAS technique using zenith-sky scattered sunlight spectra to retrieve NO_2 column densities. The required position and movement information were recorded simultaneously by a Global Positioning System (GPS) device. We performed the mobile DOAS field observations on 38 days by encircling along the IRVR in Shanghai, in fall of 2009 (pre-EXPO), spring of 2010 (opening EXPO) and fall of 2010 (closing EXPO). During the three campaigns, we derived the tropospheric NO_2 Vertical Column Densities (VCDs) and NO_x vehicle emission rates from the central urban area of Shanghai. These emissions estimates can be used for validating emission inventories and developing vehicle pollution control strategies.

2. Method and Experimental Setup

2.1. Mobile DOAS System

[6] A schematic framework of the overall mobile DOAS system is shown in Figure 1. The mobile DOAS system designed and assembled by the authors [*Wang et al.*, 2009] consists of three main parts: The first subsystem, the zenith scattered light passive DOAS is connected to the computer workstation through a USB cable. It receives the light using a telescope with 36 mm diameter and 200 mm focal length. The zenith scattered sunlight is fed to a spectrometer (B&W TEK Inc., BTC112) via a quartz fiber. This spectrometer covers the UV-VIS region (300–560 nm), allowing for the detection of chemical species with absorption features in the UV wavelengths as well as the violet and blue regions of the visible spectrum, including O_3, HCHO, HONO, H_2O, NO_2, IO, O_4 and $(CHO)_2$. The spectral resolution is about 0.65 nm full width at half maximum, as determined by calibration with a high resolution solar spectrum. The detector is a linear CCD array with 2048 pixels. The second subsystem, the GPS receiver records position and movement information such as longitude, latitude and the car speed. This information is transmitted to the computer workstation with a time resolution of 1 s. The third subsystem is the computer workstation which runs the overall system, stores the spectral and positioning data, analyses the spectra and plots the real-time track. Both the passive DOAS telescope and the GPS receiver were installed on the roof of a car.

2.2. Experimental Setup

[7] The road network of Shanghai has three concentric ring roads, i.e., the Inner Ring Viaduct Road (IRVR), the Middle Ring Viaduct Road, and the Outer Ring Road, together with a crossed Yan'an Viaduct with South-North Viaduct as its arteries. Figure 2 displays the administrative division of Shanghai and the IRVR. Embracing three districts and passing through six districts, the IRVR is regarded as the boundary of the central urban area of Shanghai. The 48 km-long IRVR can be divided into three parts: 33 km in Puxi, 11 km in Pudong and 4 km of two bridges. These two bridges, named Nanpu Bridge and Yangpu Bridge, are spanning Huangpu River and connect the IRVR between the Puxi and the Pudong part. Usually it takes about 70 min to encircle the IRVR and EXPO park, at an average car speed of 55 km/h. As shown in Figure 2b, we turned right to encircle the EXPO park after passing across the Nanpu Bridge for the first time, and then went ahead along the IRVR after passing through the Nanpu Bridge for the second time.

[8] To avoid the interference of local emission on the encirclement path during the traffic rush hours, we performed the mobile observations along the IRVR around noon time (i.e., usually between 10 A.M. and 1 P.M.) during the three campaigns. The mobile passive DOAS instrument was carrying out automated measurements by a control program FudanDOAS (Bin Zhou, Fudan University) that helps collect spectral information and store the spectra every minute. Also calibration steps such as dark current and electronic offset correction were performed by the program before spectra fitting. Associating the retrieved NO_2 VCDs with positioning data at the same time, the program FudanMobileDOAS (F. Qi, Electronic Engineering Institute, personal communication, 2009) generates color coded air quality maps illustrating the spatial distribution of NO_2 VCDs (e.g., Figures 8b and 8d).

2.3. Data Analysis and Emission Calculation

2.3.1. Spectra Analysis

[9] NO_2 column densities were retrieved from the zenith-sky spectra with the WinDOAS software [*Fayt and Van*

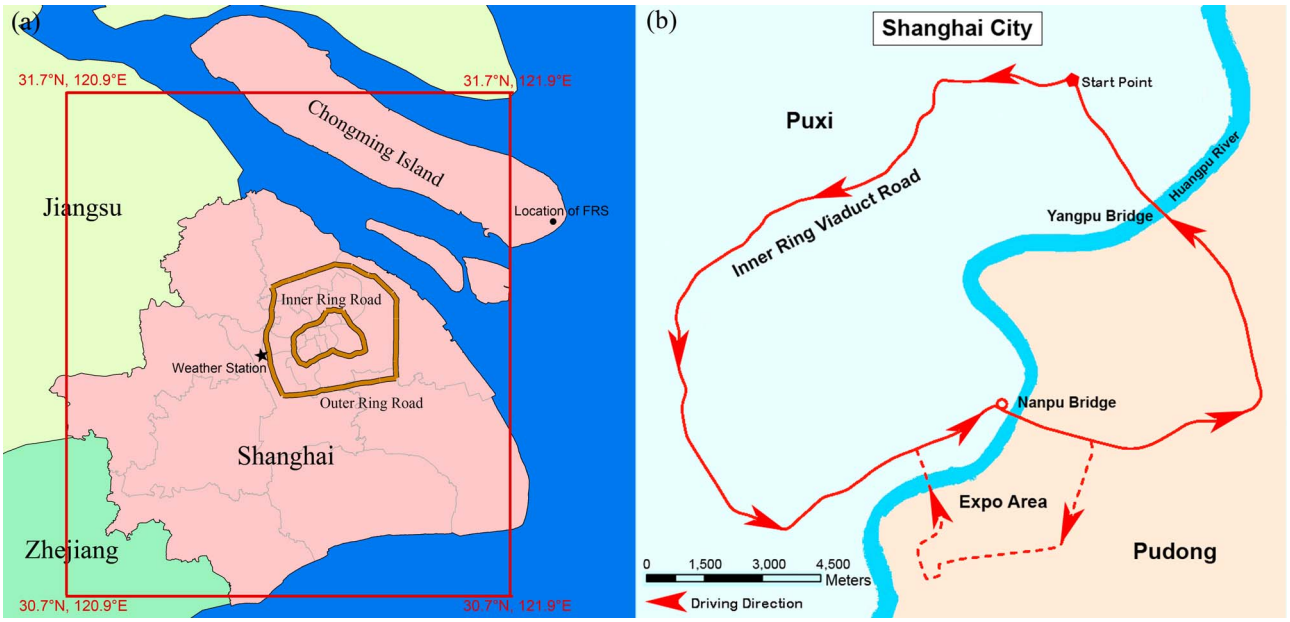

Figure 2. Administrative division of Shanghai and driving route of mobile DOAS measurements. (a) The Inner Ring Viaduct Road and Outer Ring Road, as well as the locations of Fraunhofer Reference Spectrum (FRS) and the weather station (marked with a star). (b) Driving route along the Inner Ring Viaduct Road and road encircling the EXPO park.

Roozendael, 2001] in the wavelength range of 438–457 nm. The high resolution absorption cross sections of NO_2 [*Burrows et al.*, 1998], O_3 [*Burrows et al.*, 1999], O_4 [*Greenblatt et al.*, 1990], and H_2O from the HITRAN database [*Rothman et al.*, 1998] were used in the DOAS fit. Moreover, a synthetic Ring spectrum is included in the fitting.

[10] For spectral analysis, each measured zenith-sky spectrum is divided by a relative "clean-air" spectrum, the so-called Fraunhofer reference spectrum. The reference spectrum was collected with the same spectrometer at Chongming Island on 17 April 2010 at 10:07 local time (See "location of FRS" in Figure 2a). Afterwards the output of the WinDOAS evaluation yields the Differential Slant Column Densities (DSCDs) of NO_2 between the measured and the chosen reference spectrum, as well as the uncertainties of retrieved DSCDs. The typical uncertainties of retrieved NO_2 DSCDs were estimated to be about 10% [*Ibrahim et al.*, 2010; *Rivera et al.*, 2009; *Shaiganfar et al.*, 2011]. An example of a NO_2 DOAS-fit result is shown in Figure 3.

2.3.2. Tropospheric NO_2 VCDs

[11] Considering the special geographic location and good long-term air quality of the Chongming Island, the NO_2 values from this reference spectrum can be taken for the background values of stratospheric NO_2 over Shanghai with the approximation that the reference spectrum would be free of tropospheric NO_2 [*Chen et al.*, 2009]. A typical total NO_2 column of 5×10^{15} molec/cm^2 for the Chongming Island has been verified in previous measurements e.g., in December 2006, November 2009 and April 2010. Therefore, the retrieved DSCDs are expected to be the tropospheric NO_2 slant column densities. Compared to the high polluted tropospheric NO_2 in central urban area, we neglected the relatively small tropospheric NO_2 pollution contained with the reference spectrum. An Air Mass Factor (AMF) is applied to convert the DSCD to the VCD.

$$VCD_{trop} = \frac{SCD_{trop}}{AMF_{trop}} = \frac{DSCD}{AMF_{trop}}. \quad (1)$$

[12] Note that in previous studies [e.g., *Johansson et al.*, 2008, 2009; *Rivera et al.*, 2009, 2010] the light path has been assumed to be vertical and the DSCDs were used directly for emission calculation without AMFs conversion. Here we calculated the tropospheric NO_2 AMFs for the central wavelength (447 nm) of the fitting range with the radiative transfer model SCIATRAN 2.2 [*Institute of Remote Sensing*, 2007]. The monthly and latitudinally dependent vertical distribution profiles for pressure, temperature and ozone at 30°N–40°N are taken from the McLinden climatology contained in SCIATRAN database [*McLinden et al.*, 2002]. A single priori NO_2 profile is used with a constant concentration of 5.4×10^{11} molecules cm^{-3} (equal to 20 ppb at the ground level) within the boundary layer (BL) of 800 m [*Chen et al.*, 2009]. The urban aerosol is assumed to be in homogenous layers extending from the surface to the top of BL, following an exponential decrease with height [*Leitão et al.*, 2010]. Here the urban aerosol loads is adopted with representative aerosol optical depths (AOD) of 1.0 and 0.7 for spring and autumn, respectively [*Pan et al.*, 2010].

[13] Since the tropospheric AMFs is largely dependent on aerosol and NO_2 content in BL, we attempted to estimate the uncertainties in AMF with a sensitivity study by varying the setting of boundary layer height (BLH), aerosol and NO_2 loading. To simplify, we assumed that the majority of anthropogenic sources are the same for both NO_2 and aerosols. Therefore, they would have similar spatial distributions

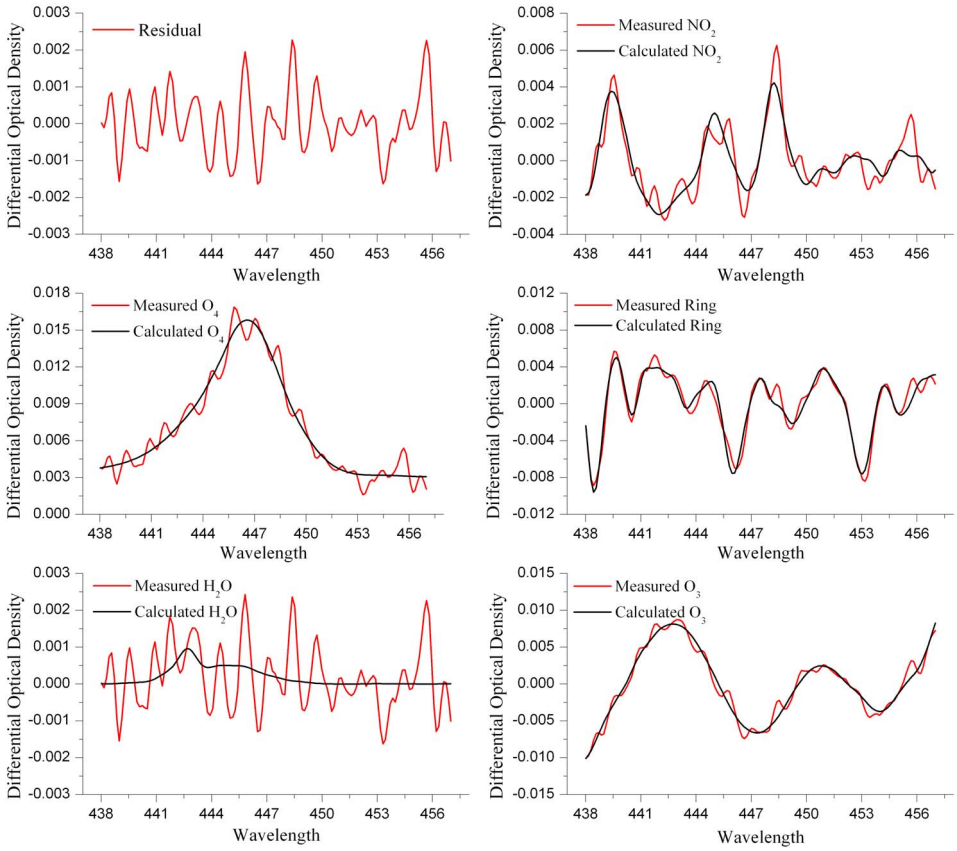

Figure 3. Example of the DOAS NO_2 fit in the 438–457 nm wavelength range (NO_2 2.46 × 10^{16} molec/cm^2). (top) The residual of the fit and NO_2 (293 K) fitted cross section; (middle) the fit of O_4 and the synthetic ring spectrum; and (bottom) fits for H_2O and O_3 (223 K). The measured spectrum was collected on 4 October 2009 at 11:26 local time (E 121.50, N 31.19).

of simple box profile with BL. The tropospheric NO_2 AMFs, simulated with a layer (aerosol and NO_2) height of 800 m, AOD of 0.7 and NO_2 concentration of 20 ppb, were selected as the reference scenario. A set of input parameters for NO_2 and aerosol were attempted as sensitive cases. The AODs were adopted with range of monthly values in Pudong reported by *Pan et al.* [2010], whereas the BLHs were set in accordance with the monthly and diurnal variation in Shanghai [*Yang et al.*, 2006]. Besides, we referred to the measured NO_2 concentrations to mount the NO_2 loads in BL. The results of the uncertainties in AMF under such assumptions are detailed below.

[14] The tropospheric NO_2 AMFs calculated under the same scenario of BLH and moderate polluted NO_2 but different AODs of spring and autumn were shown in Figure 4a. The results reveal the difference between the marine aerosol, which is composed of water soluble aerosol, coarse and accumulation mode sea-salt, and the pure dust aerosol. The AMFs resulting from the simulations with fine aerosols with different AODs are similar, which are much higher than those of coarse particles (dust aerosol). Figure 4b displays the tropospheric NO_2 AMFs deduced from different assumed AODs (0.5, 0.7, 1.0, and 1.2) and moderate polluted NO_2 with a BLH of 800 m. Higher AOD presents larger tropospheric NO_2 AMFs when the SZA is less than 60°. The errors caused by an assumed uncertainty of AOD in a range of 0.5 to 1.2 are less than 10%. Given the AOD of 0.7 and moderate polluted NO_2, but different BLHs of 600, 800, 1000, 1200, and 1500 m, the results shown in Figure 4c indicate that the tropospheric NO_2 AMFs are sensitive to the BLH, especially for the 10% regression in AMFs caused by the increase of BLH from 600 to 800 m. Moreover, the influences of NO_2 pollution on tropospheric NO_2 AMFs are investigated for heavy, moderate and light polluted NO_2 of 50, 20 and 5 ppb with a BLH of 800 m and AOD of 0.7. As demonstrated in Figure 4d, the uncertainties of AMFs caused by different NO_2 amount, increased with SZAs, and were up to 15% for SZAs larger than 60°.

[15] Though the respective uncertainties in groups of cases are up to 10%, we estimated the total uncertainties of tropospheric NO_2 AMFs to be 20–30% because of smaller errors for SZAs less than 40°, i.e., during noontime when the mobile DOAS observation were usually performed.

[16] The presence of clouds was not taken into account in above cases, which could bring uncertainties to the results. In order to reduce the interference of clouds, we screened the cloudy days via the meteorological data and the retrieved O_4 DSCD. Since the atmospheric O_4 concentration profile is well known and nearly constant, the observed O_4 absorption clearly indicates the atmospheric distribution of photon paths [*Wagner et al.*, 2004]. For example, due to the multiple Mie scattering inside the clouds, the increased geometrical path length enhances both the absorptions of O_4 and H_2O largely. Accordingly, 14 days are excluded from the

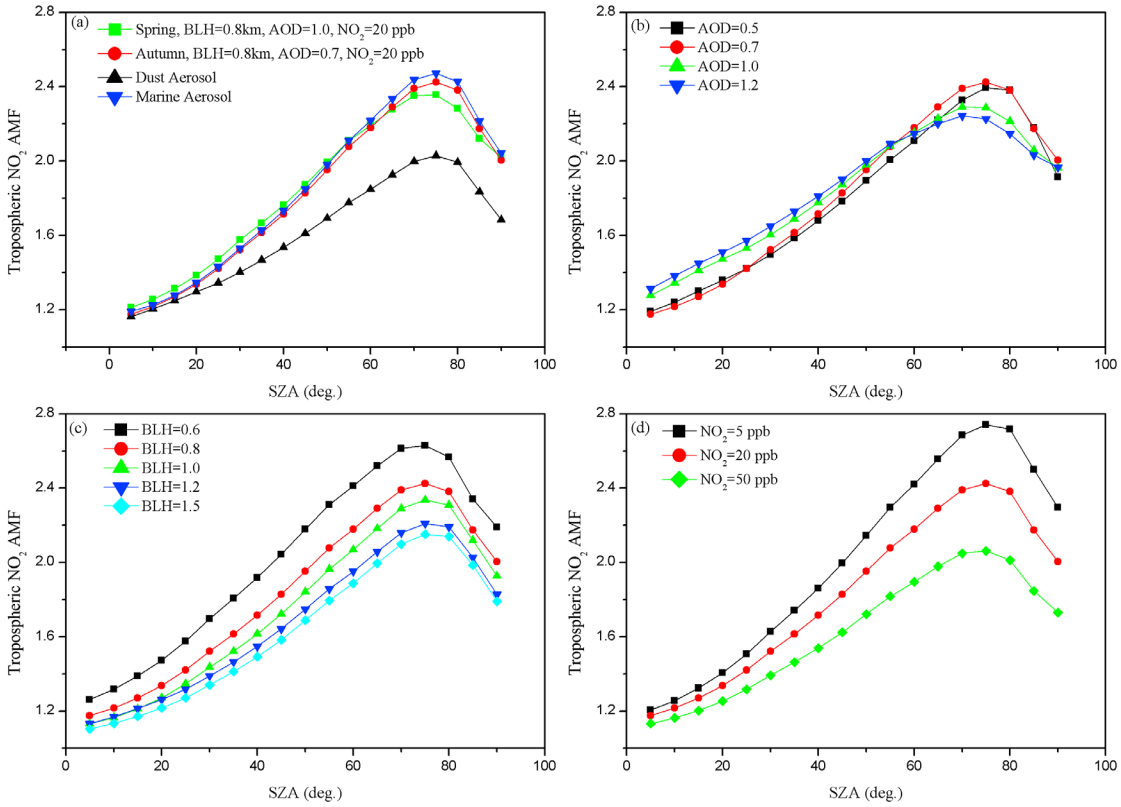

Figure 4. Case study of the influence of BLH, aerosol and NO_2 loading on the tropospheric NO_2 AMFs, modeled with SCIATRAN. The tropospheric NO_2 AMFs deduced under the assumption (a) that seasonal characteristics and different aerosol constituent, (b) of different AOD, (c) of different BLH, and (d) of different pollution circumstances.

emission calculation because of their large O_4 absorption and drastic variation of O_4 absorption during the encirclement, i.e., 29 and 30 September, 1, 7 and 9 October 2009, 5, 7 and 9 May, 25, 26, 29 and 30 October, 1 and 2 November in 2010.

2.3.3. Emission Calculation

[17] Generally, the continuity equation for emission calculation involves three terms: source, flux divergence, and rate of change of concentration:

$$\frac{\partial \varphi}{\partial t} + \nabla \cdot \vec{f} = \sigma. \tag{2}$$

[18] Where φ is the trace gas amount, $\vec{f}$ is a vector function describing the flux (flow per unit area and unit time) of φ, $\nabla \cdot \vec{f}$ is divergence of the vector field $\vec{f}$, t is time, and σ is the generation (or removal) per unit volume and unit time of φ. Terms that generate ($\sigma > 0$) or remove ($\sigma < 0$) φ are referred to as a "sources" and "sinks" respectively.

[19] To simplify, we neglected the time derivation of total NO_2 amount ($\frac{\partial \varphi}{\partial t}$) in the continuity equation and expressed the continuity equation in integral form. The consideration of whether it is appropriate to be neglected will be detailed in Section 3.4. Therefore, the total flux, which is the difference between the fluxes entering and leaving the encircled area, can be determined by taking the integral along the driving route [*Ibrahim et al.*, 2010; *Johansson et al.*, 2008].

$$F_{total} = \int_A div\left(VCD \cdot \vec{W}\right) dA = \oint_S VCD(s) \cdot \vec{W} \cdot \vec{n} \cdot ds. \tag{3}$$

[20] The angle $\alpha(s_i)$ between the driving direction and the wind direction has been introduced in discrete steps in order to distinguish the flux entering or leaving the encircled region, in upwind and downwind flow. Consequently the total NO_2 emission within the IRVR can be described as follows:

$$\begin{aligned} F_{NO_2} &= \sum_i F_{iNO_2} = \sum_i VCD_{NO_2}(s_i) \cdot \vec{W} \cdot \vec{n} \cdot \Delta s_i \\ &= \sum_i VCD_{NO_2}(s_i) \cdot W \cdot \sin\alpha(s_i) \cdot \Delta s_i. \end{aligned} \tag{4}$$

[21] In equation (4), the NO_2 VCD, i.e., the integral of the concentration along a vertical line from the instrument and up, has been determined for each finite path element s_i (between the starting points of two successive measured spectra along the IRVR). $\vec{n}$ represents the normal vector parallel to earth's surface and orthogonal to the driving direction. $\vec{W}$ is the average wind vector for each IRVR encirclement. Δs_i is the

geometric distance between the locations at the beginning of two successive spectra measurements.

[22] The total NO_x (=NO+NO_2) emission rate can be inferred from the NO_2 emission rate using two correction factors, the ratio (R) of NO/NO_2 and the NO_x lifetime correction (c_t):

$$F_{NO_X} = (1 + R) \cdot c_t \cdot F_{NO_2}. \quad (5)$$

[23] Here $1 + R$ is a correction factor based on the assumption that a partitioning of NO_x into NO and NO_2 occurs. The ratio of NO/NO_2 is determined by dynamic chemical reactions and is difficult to grasp without a direct measurement. *Geng et al.* [2008] reported that the NO/NO_2 ratio varied from 0.6 to 1.1 in summer 2006 and from 0.3 to 0.5 in winter 2007, which was measured in the central urban area of Shanghai during the identical periods between 10 A. M. and 1 P.M. local time. We adopted the typical NO/NO_2 ratio of 0.6 in emission calculation. Hereby, the uncertainties in emissions are estimated to be 20–30% considering the seasonal variations of the NO/NO_2 ratio.

[24] The NO_x lifetime varies from a few hours to a couple of days depending on the OH and ozone concentrations via complex chemistry mechanisms, as well as on the aerosol load, the NO/NO_2 ratio, and the meteorological conditions and photolysis strength [*Atkinson*, 2000]. c_t is a correction factor accounting for the destruction of NO_x and the NO_x lifetime in the urban environment at noon time:

$$c_t = e^{\frac{D/W}{t}}. \quad (6)$$

[25] Assuming that the NO_x is emitted from the center of the IRVR, it would take between 20 and 60 min to be transported from the center to the measurement location on the IRVR based on the average distance (D) of the emission source from the measurement location and the average wind speed (W) for individual encirclements. The resulting c_t is in the range of 1.04–1.24 under the assumption of a typical NO_x lifetime (t) of 5 h for polluted areas in East China [*Lin et al.*, 2010; *Shaiganfar et al.*, 2011]. Given the high OH concentrations and the short NO_x lifetime in urban plumes at noon, the NO_x loss may be underestimated. Nevertheless, the uncertainty in NO_x lifetime is probably of secondary concern for the time scales involved in the measurements (typically less than one hour). The uncertainty in emissions due to the variations of the correction factor c_t caused by NO_x lifetime and wind speed is estimated to be about 10–15%.

2.4. Wind Field

[26] The wind data used in this study were obtained from the automatic weather station located at Hongqiao airport, Shanghai (31.20°N, 121.34°E, station elevation above m.s.l. 3 m). The wind direction and speed at 10 m height were given every 30 min. We averaged the wind direction and speed during the period of an encirclement. The mean value and standard deviations of the wind parameters for the 38 round trip encirclements are listed in Table 1. Relatively stable wind field before and during the measurements is prerequisite for making the flux measurements by the mobile DOAS method [*Johansson et al.*, 2008]. For single encirclement, the standard deviations of wind speed are generally small compared to the absolute mean value, as well as the standard deviation of wind direction. The uncertainties in the wind field at 10 m were estimated to be 10–20% based on the standard deviations of ~15° in wind direction and of ~10% in the wind speed.

[27] Besides the wind data fluctuations in the encirclement duration, errors caused by wind field are related to wind vertical profile. Since the emissions will be distributed throughout the BL, the wind field at higher altitude would be much relevant to the emission estimation. According to the 15 years meteorological observation, the monthly BLH in Shanghai has been reported varying within a small range from 500 to 700 m. The seasonal variation of BLH was characterized with relatively larger value in summer and smaller value in winter, as well as an approximately moderate value in spring and autumn. Considering the diurnal variation, the BLH around noontime would be assumed to 800 m, as it increased from 300 m at 02:00 to 900 m at 14:00 [*Yang et al.*, 2006]. We compared the wind data of atmospheric sounding at ground surface to 800 m height at Baoshan meteorological site (31.40°N, 121.46°E) in Shanghai (http://weather.uwyo.edu/upperair/sounding.html). Figure 5 illustrates that the wind directions at BLH ~800 m are much close to those at 4 m in majority cases, with relative deviation of ~20°. In contrast, wind speeds at 800 m have commonly doubled or tripled, as against that at ground surface.

[28] As a result, the effective wind speed relevant to the NO_2 layer is probably underestimated if the wind data at 10 m are only compelled to be used. Since the vertical mixing occurs quickly in the BL, the middle height of BLH, i.e., 400 m, was taken as the representative horizontal transport height under an assumption that the emissions were expected to be well mixed throughout the whole BL around noontime. The wind velocity in lower atmosphere (<1000 m) is obedient to the increased with the height by power function. By the power function fitting for the daily atmospheric sounding data at Baoshan site, we calculated the ratios of wind speeds at 400 m to that at 10 m, with an average of 1.34. Since no real time atmospheric sounding data of the mobile measurement duration was available, we used a coefficient of 1.34 to multiply the wind speed at 10 m in order to compensate the underestimation in emission estimation. Thus the underestimation of the determined emission rates will be small and acceptable. Together with the uncertainties of wind field variation in vertical using the exponential factors to calculate wind speed at 400 m, we estimated that the uncertainties in emission caused by wind data would be 20–30%.

3. Results and Discussion

3.1. Daily NO_2 Vertical Column Densities

[29] According to the retrieval procedure described in Sections 2.3.1 and 2.3.2, we derived the NO_2 VCDs along the route for each encirclement. As shown in Figure 6, the averaged NO_2 VCDs varied from $(18.4 \pm 4.4) \times 10^{15}$ to $(98.8 \pm 5.2) \times 10^{15}$ molec/cm^2 during the three campaigns, with a mean value of $(37.0 \pm 4.5) \times 10^{15}$ molec/cm^2 during the EXPO period (blue rectangle in Figure 6). The so-called "holiday effects" can be observed, i.e., as a result of less

Table 1. Summary of the Daily Number of Finite Path Elements, Start-End Time of Encirclement, Wind Data at 10 m Height From Hongqiao Between 10 A.M. and 1 P.M.

Date	Time	FPE[a]	Wind Direction[b] (deg)	Wind Speed (m/s)	$\Delta VCD_{down-up}$ (10^{15} molec/cm^2)	Flag[c]
2009-9-29	10:33–12:42	98	48.75 ± 9.19	5.5 ± 0.84		–
2009-9-30	10:46–12:55	89	75.00 ± 25.98	3.0 ± 0.82		–
2009-10-1	10:29–11:44	48	28.13 ± 11.25	5.0 ± 0.82		–
2009-10-2	10:55–12:28	66	348.75 ± 12.99	4.75 ± 0.50	3.8	–
2009-10-3	10:51–12:14	54	84.38 ± 11.25	3.0 ± 0.00	8.9	Yes
2009-10-4	10:39–12:02	50	95.63 ± 11.25	3.2 ± 0.84	12.0	Yes
2009-10-5	10:43–12:04	54	49.50 ± 10.06	3.8 ± 0.45	−5.2	–
2009-10-6	10:37–11:53	50	39.38 ± 11.25	6.5 ± 0.58	5.3	Yes
2009-10-7	10:37–12:03	55	27.00 ± 10.06	7.6 ± 0.55		–
2009-10-8	10:50–12:08	46	0.00 ± 0.00	5.0 ± 0.71	6.0	Yes
2009-10-9	10:53–12:09	50	40.50 ± 18.82	3.2 ± 0.45		–
2009-10-10	10:55–12:16	53	56.25 ± 22.50	5.4 ± 0.55	8.1	Yes
2010-4-29	10:43–12:16	64	189.00 ± 12.32	4.2 ± 0.84	4.7	–
2010-4-30	10:54–12:30	55	292.50 ± 59.53	2.0 ± 0.71	3.8	–
2010-5-1	10:49–12:17	55	166.50 ± 20.12	3.0 ± 1.00	1.3	–
2010-5-2	10:31–11:36	40	180.00 ± 0.00	3.75 ± 0.50	2.5	–
2010-5-3	10:47–11:58	42	140.63 ± 11.25	5.2 ± 0.50	4.7	Yes
2010-5-4	10:34–11:36	39	163.13 ± 11.25	9.0 ± 0.00	2.3	Yes
2010-5-5	10:36–11:57	56	163.13 ± 11.25	6.0 ± 0.00		–
2010-5-6	10:54–12:06	42	306.00 ± 25.65	3.6 ± 0.89	20.4	Yes
2010-5-7	10:40–12:09	60	180 ± 0.00	1.8 ± 0.45		–
2010-5-8	10:34–12:16	44	126.00 ± 12.32	4.8 ± 0.45	2.6	–
2010-5-9	10:37–12:00	52	112.50 ± 0.00	2.75 ± 0.96		–
2010-5-10	10:38–12:16	49	4.50 ± 10.06	3.8 ± 1.10	−4.5	–
2010-10-25	10:23–11:47	57	0.00 ± 0.00	9.5 ± 1.29		–
2010-10-26	10:24–11:59	60	5.63 ± 11.25	8.75 ± 1.50		–
2010-10-27	10:47–12:09	60	0.00 ± 0.00	8.6 ± 0.55	7.1	Yes
2010-10-28	10:29–11:57	62	0.00 ± 0.00	8.0 ± 0.00	9.3	Yes
2010-10-29	10:33–12:37	98	0.00 ± 10.62	7.17 ± 0.98		–
2010-10-30	10:34–12:40	70	11.25 ± 18.82	6.33 ± 0.52		–
2010-10-31	10:41–12:00	50	343.13 ± 11.25	4.0 ± 0.00	18.0	Yes
2010-11-1	10:43–11:52	46	16.88 ± 21.54	3.75 ± 0.50		–
2010-11-2	10:41–11:50	47	22.50 ± 0.00	5.75 ± 0.50		–
2010-11-3	10:29–11:53	57	315.00 ± 46.84	2.0 ± 0.00	14.7	Yes
2010-11-4	10:35–11:49	52	120.00 ± 12.99	2.25 ± 0.86	8.5	–
2010-11-5	10:51–12:02	48	135.00 ± 15.91	3.0 ± 0.00	9.8	Yes
2010-11-6	10:39–12:03	–	157.5 ± 15.91	4.0 ± 0.71		–
2010-11-7	10:26–11:36	47	253.13 ± 11.25	2.5 ± 0.58	8.2	Yes

[a]A finite path element is defined to be the traversed cross section between the starting points of two successive measured spectra.
[b]Wind direction was given clockwise by 16 cardinal directions, e.g., wind from north is 0° (N), wind from east is 90° (E).
[c]Flag for days to be estimated (Yes) or skipped (–).

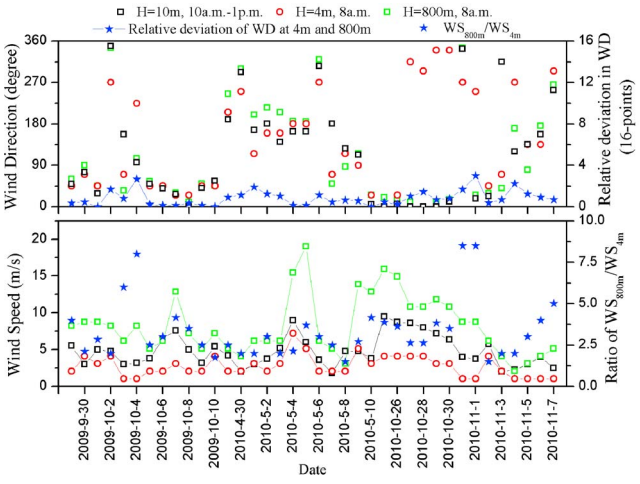

Figure 5. The comparison of wind direction and speed at ground surface and 800 m height from atmospheric sounding at Baoshan meteorological station in Shanghai.

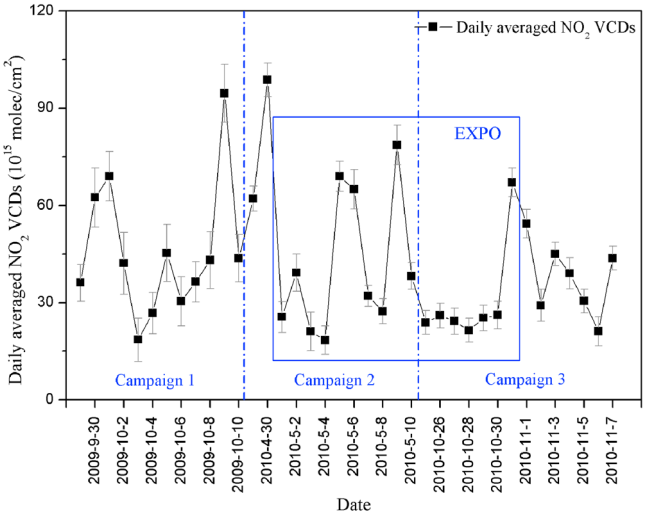

Figure 6. Averaged NO_2 VCDs along the route measured by mobile DOAS for each IRVR encirclement during the three campaigns. The EXPO period is denoted by a blue box.

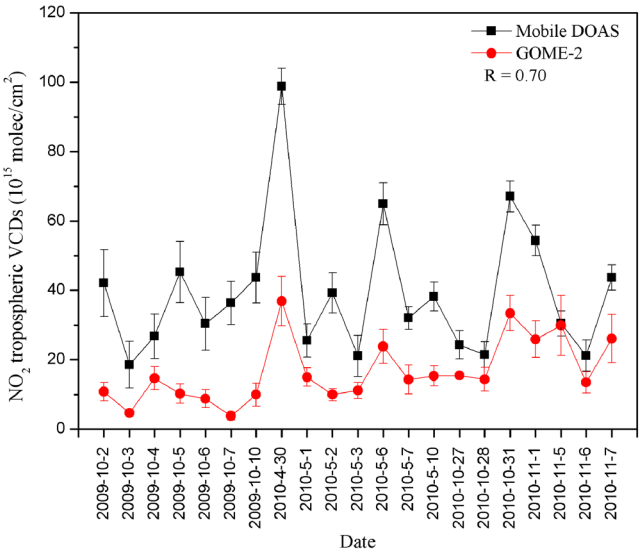

Figure 7. Comparison between daily tropospheric NO_2 VCDs measured by mobile DOAS along the encirclement route during three campaigns and daily average GOME-2 VCDs for the region in Figure 2 denoted by the red rectangle.

traffic, the averaged NO_2 VCD of $(34.6 \pm 6.9) \times 10^{15}$ molec/cm^2 during the holiday periods from 1 October to 8 October in 2009 and from 1 May to 4 May in 2010 is relatively small compared to that on working days $(45.6 \pm 4.8) \times 10^{15}$ molec/cm^2. This indicates that vehicles are a major source of anthropogenic NO_2 in the central urban area.

[30] The NO_2 VCDs from the mobile DOAS measurements along the IRVR have been compared with satellite observations from the Global Ozone Monitoring Experiment-2 (GOME-2). GOME-2 is a nadir-scanning UV-VIS spectrometer with a spectral coverage of 240–790 nm and a spectral resolution between 0.26 and 0.51 nm. It has a spatial resolution of 80 × 40 km^2, and provides a global coverage within about 1.5 days [*Munro et al.*, 2006]. Operational tropospheric NO_2 products are provided by the German Aerospace Center (DLR) in the framework of the O3MSAF [*Valks et al.*, 2011a, 2011b]. Daily averaged GOME-2 tropospheric NO_2 VCDs were obtained by averaging all GOME-2 measurements with cloud fraction <0.2 within the region covering Shanghai (30.7–31.7°N, 120.9–121.9°E, red rectangle in Figure 2a). Because of the large pixel size of GOME-2, we have to choose a rather large area (Shanghai and its surrounding areas) for comparison. If we only choose one pixel or a smaller region with a few pixels only, then there remain only a few days for the comparison after the cloud screening. Figure 7 shows the absolute values of tropospheric NO_2 VCDs from mobile DOAS measurements and GOME-2 data. The relative variations of these two data sets match quite well with a correlation coefficient of 0.70. The large difference in the absolute value of tropospheric NO_2 VCDs between mobile DOAS measurements and GOME-2 observations is mainly due to the differences in the spatial resolution of the two observation techniques. The central urban area encircled by the mobile DOAS field measurements undergoes heavy local NO_2 pollution from vehicle emissions, whereas the satellite measurements additionally cover the much less polluted area outside the IRVR.

3.2. NO_2 Variation Along IRVR

[31] To illustrate the spatial distribution along the IRVR, we show the NO_2 VCDs on a pre-EXPO day (6 October 2009) and the EXPO opening ceremony day (1 May 2010). Figure 8a shows how NO_2 VCDs vary with time during the encirclement on 6 October 2009. A map of NO_2 VCDs along the route is shown in Figure 8b. The main peak values of NO_2 VCDs usually occurred at traffic congested junctions of the IRVR with other main roads, such as at the Gonghexin Road junction, the West Yan'an junction, and the Caoxi junction. The peak values in Figure 8a correspond to the location of Gonghexin Road junction (Peak 1 with $(54.4 \pm 5.6) \times 10^{15}$ molec/cm^2) and the section from West Yan'an junction to Caoxi junction (Peak 2 with $(69.8 \pm 7.0) \times 10^{15}$ molec/cm^2). Both the higher traffic volume and the condition under which the vehicles were operated (rapid acceleration or deceleration, etc.) were responsible for the peak values at these junctions. On the EXPO opening ceremony day 1 May 2010, the NO_2 VCDs for the entire IRVR showed a smaller variation ranging from $(18.5 \pm 2.5) \times 10^{15}$ molec/cm^2 to $(34.8 \pm 3.7) \times 10^{15}$ molec/cm^2, as displayed in Figures 8c and 8d. In contrast to the encirclement on 6 October 2009, NO_2 emitted from vehicles spread all over the area without showing a predominant peak value. The absence of peak values on 1 May 2010 can be attributed to the traffic restrictions applicable at the time of the EXPO opening ceremony, as well as the "holiday effects."

[32] As shown in Figures 8b and 8d, the average NO_2 VCDs in the Pudong part are lower than in the Puxi part during the three campaigns. Besides influences by traffic conditions, this could be due to the fact that the building density in Pudong district is 20% lower than that in the other urban districts where IRVR passes through. Fewer buildings, together with lower building height near IRVR in Pudong, may facilitate the airflow thus the diffusion of pollutants. Furthermore, the roadside trees and greenbelts along the IRVR may have effects on the diffusion of NO_2.

[33] Besides the traffic volume and vehicle operating condition mentioned above, the wind direction and speed have a strong effect on the NO_2 spatial distribution too. The downwind NO_2 VCDs are usually higher than the corresponding upwind values in most cases, as shown in Figure 9a. Figure 9b shows the ratio of the downwind and upwind NO_2 VCDs as a function of wind direction. It can be seen that all cases for which the upwind values are higher than the downwind values occurred under northerly wind. Wind speed can greatly affect the pollutant concentration since wind dilutes and disperses pollutants throughout the immediate area. There is an inverse relationship between wind speed and pollution, i.e., the higher the wind speed the lower the pollutant concentration. Figure 10 shows the relationship between the daily mean NO_2 VCDs along the IRVR and the wind speed during the three campaigns. A clear positive correlation is found between the reciprocal of the wind speed and NO_2 VCDs for wind speed larger than 4 m/s (R = 0.82).

3.3. Investigation for EXPO

[34] Figure 8 shows that NO_2 VCDs of the road surrounding the EXPO park are typically the lowest of the total encirclement (red part in both Figures 8a and 8c). For further

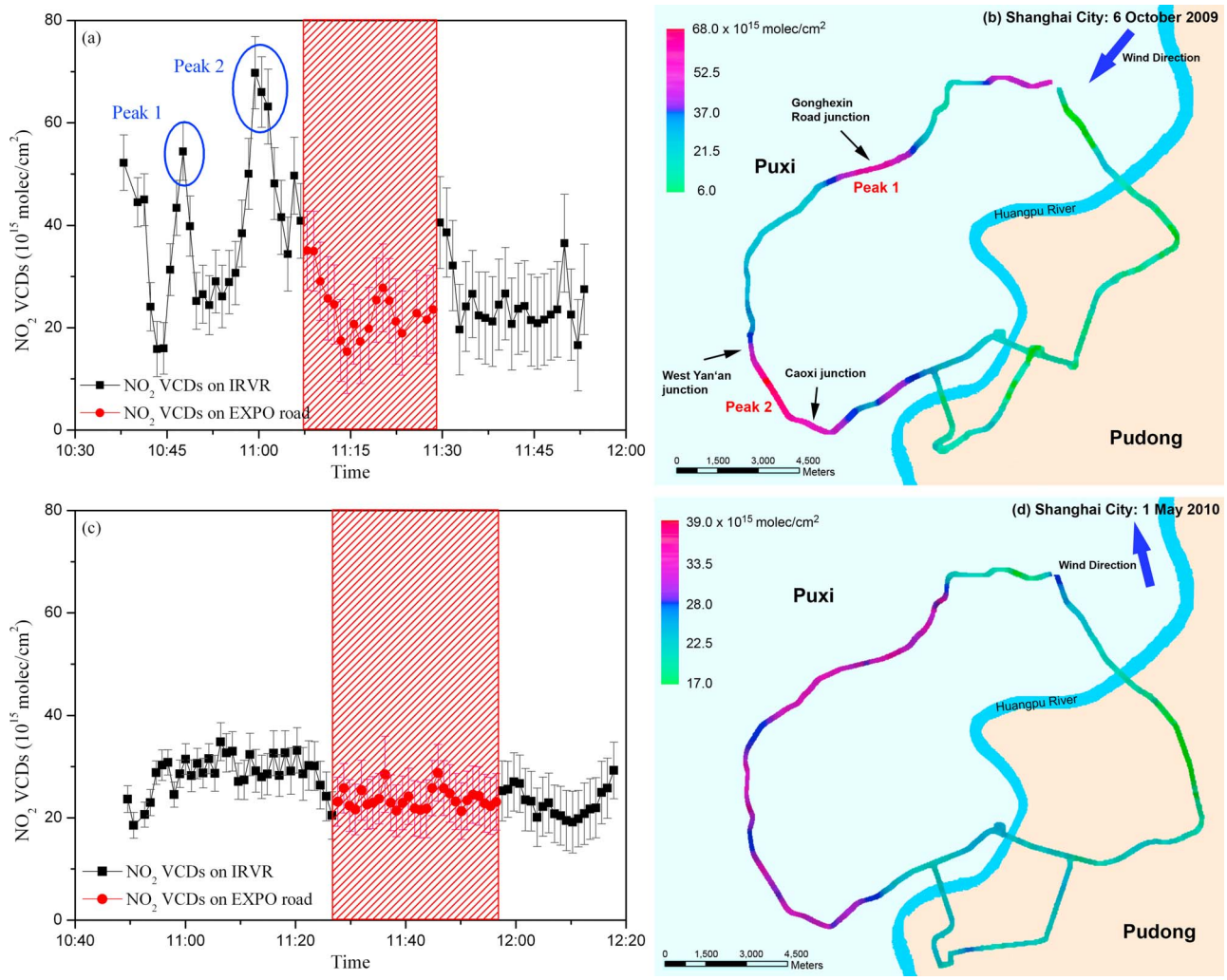

Figure 8. NO_2 VCDs along the IRVR. (a) The variation of NO_2 VCDs with time and (b) the spatial distributions of NO_2 VCDs on 6 October 2009 from 10:37 to 11:54 local time based on interpolation management, respectively. The (c) temporal NO_2 VCDs variation and (d) spatial distribution on 1 May 2010 from 10:49 to 12:18 local time. The red hatched area shows the EXPO park encirclement.

comparison, Figure 11 illustrates the daily mean NO_2 VCDs of the EXPO park road and IRVR. Due to the higher density of roads and traffic volume, daily VCDs at the IRVR are on average 20% larger than on the EXPO park road during the EXPO time in most cases, with peak values reaching almost twice as much. The IRVR/EXPO ratios during the pre-EXPO period of Campaign 1 vary from about 0.6 to 1.8 due to the absence of measures of air pollution reduction in EXPO park, whereas the daily NO_2 VCDs ratios of IRVR and EXPO park road are mostly above 1.0 during the Expo period. Similarly, the difference has apparently been reduced during the post-EXPO period. This could be attributed to the fact that the traffic restrictions and controls within the EXPO park were no longer applicable after the EXPO had ended.

[35] To investigate the air quality at the EXPO park, averaged in situ NO_2 concentrations measured in EXPO park for the duration that mobile DOAS measurements encircled the EXPO park have been compared with the daily averaged VCDs at the EXPO park road. This in situ monitoring system belonged to the air quality monitoring network for EXPO park and surrounding areas. The network, including one stationary station and three road chambers inside EXPO park, was managed by the Shanghai Environmental Monitoring Centre (SEMC). As shown in Figure 12, there exists a very good correlation between the mobile DOAS and in situ instrument data sets during EXPO period (R = 0.89), which could be interpreted by that the observation durations of them are similar and observation sites are closer.

3.4. NO_2 Emission From IRVR

[36] Before the emission estimation, we should consider whether the time derivative of NO_2 concentration in equation (2) can be neglected. The condition to justify the neglect of the time derivative is:

$$\frac{dVCD_{inside}}{dt} \ll \frac{\Delta VCD_{down-up}}{tau} \tag{7}$$

where VCD_{inside} typifies the NO_2 amount inside the IRVR, $\Delta VCD_{down-up}$ is the change in VCD from upwind to

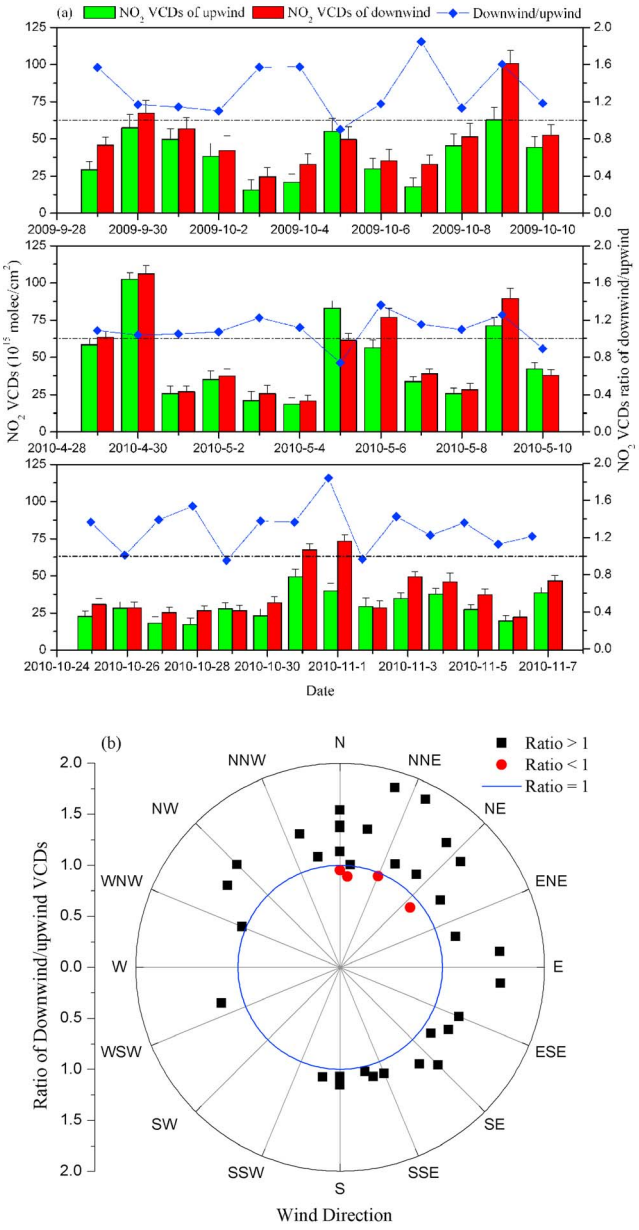

Figure 9. (a) Daily average NO_2 VCDs for the upwind and downwind parts of the IRVR, as well as (b) the ratio of downwind/upwind NO_2 VCDs as a function of wind direction.

downwind, and the *tau* is the time it takes air to advect across the ring. The equation (7) can be expressed as the concentration increase:

$$\frac{dN}{dt} \ll \frac{\Delta VCD_{down-up} \cdot W}{H \cdot L} \tag{8}$$

where N is the NO_2 concentration, L is the distance across the ring, H is the height over which the emissions are distributed, and W is the wind speed.

[37] It is difficult to consider the absolute value of each side simultaneously. For the left side of the inequation, no measured data about the change of NO_2 concentration for our observation duration is available. The diurnal NO_2 tendency in Shanghai urban area has been reported by *Geng et al.* [2008], which is smaller than 2 ppbv/h during noontime between 11 A.M. and 1 P.M.. For the right side, this inequation will not be satisfied if the wind speed is not large enough, likewise the $\Delta VCD_{down-up}$. Besides, the inequation is dependent on the distance across the ring and the height over which the emission are distributed.

[38] Referring to the NO_2 increase of 2 ppbv/h, given the typical values of L and H, the wind speed should be larger than 10 m/s to neglect the time derivative under a moderate $\Delta VCD_{down-up}$ of about 4×10^{15} molec/cm^2. Conversely, at moderate velocity of 5 m/s and the extreme small velocity of 1 m/s, the NO_2 increase rate must be smaller than 1.0 and 0.2 ppbv/h, respectively. Since both $\Delta VCD_{down-up}$ and wind speed have strong influences on the justification, the product of $\Delta VCD_{down-up} \cdot W$ larger than 20×10^{15} molec/cm^2·m/s can be defined as the criterion to justify the neglect of the time derivative in the continuity equation. It is worth pointing out that this selection criterion possibly causes high-biased emission estimation due to eliminating the lower part of the statistical distribution of actual fluxes either for a constant emission source or for a source with natural variability.

[39] Based on the above considerations, we skipped those inappropriate days in which the time derivative cannot be neglected, i.e., 2 and 5 October 2009, 29 and 30 April, 1, 2, 8 and 10 May, 4 and 6 November in 2010. Finally, we derived NO_2 fluxes at each finite path element, integrated total NO_2 emissions within the IRVR using equation (4) for the 14 remaining days. The strength of vehicle emissions within the IRVR is much higher than for the outside downtown area as a result of the high traffic volume and higher road densities. As a consequence, most of the calculated daily total NO_2 emissions are positive, indicating that the large area source encircled by the IRVR emits pollutants to the outside. Estimates of the average NO_2 emissions amount to 2.1 ± 0.9 ton/h, 2.8 ± 1.4 ton/h, and 2.7 ± 1.4 ton/h for the three campaigns.

[40] Considering the ideal case that a single traverse of NO_2 plume is perpendicular to the wind direction and significant NO_2 column were assumed to be only detected on the upwind and downwind legs of the circular mobile DOAS route, the error of NO_2 flux for each finite path element (i) through the area above the instrument is given by:

$$\frac{\Delta F_{iNO_2}}{F_{iNO_2}} = \sqrt{\left(\frac{\Delta AMF}{AMF}\right)_i^2 + \left(\frac{\Delta \vec{W}}{\vec{W}}\right)_i^2 + \left(\frac{\Delta DSCD}{DSCD}\right)_i^2}. \tag{9}$$

[41] Where the error of Δs_i was negligible due to the high accuracy of the GPS. Furthermore, the relative error of the NO_2 emission rate from the IRVR, which is dependent on the error propagated from each finite path element, is determined via:

$$\frac{\Delta F_{NO_2}}{F_{NO_2}} = \frac{\sqrt{\sum_i \Delta F_{iNO_2}{}^2}}{\sum_i F_{iNO_2}}. \tag{10}$$

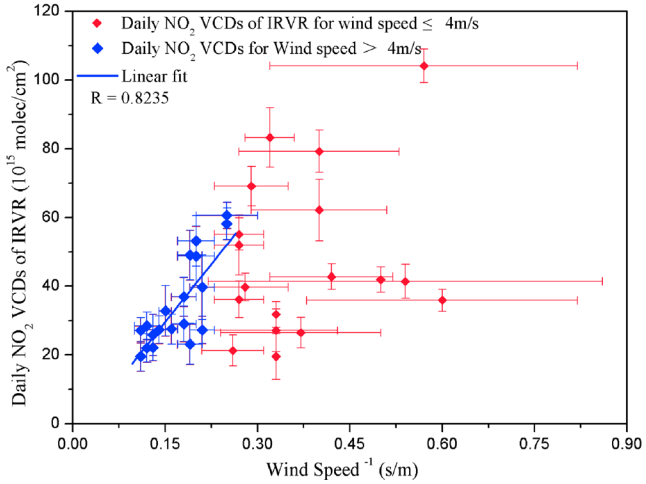

Figure 10. Statistical analysis of daily mean NO_2 VCDs along the IRVR and the reciprocal of the wind speed during the three campaigns. The red diamonds show the daily NO_2 VCDs for wind speed ≤4 m/s. The blue diamonds show the daily NO_2 VCDs for wind speed >4 m/s.

[42] For those remaining days to be estimated, the uncertainties on tropospheric NO_2 AMFs are supposed to be about 20–30% after correcting via the O_4 absorption. And the error on the wind speed and direction was estimated to be 20–30%. The typical uncertainties of retrieved NO_2 DSCDs are estimated at about 10%. Accordingly, the error of the final average NO_2 emission rates obtained was 45% for several consecutive days.

3.5. Vehicle Emission and Comparison With Emission Inventories

[43] According to equation (5), the NO_x emissions were inferred from the estimated NO_2 emissions using a c_t calculated for every encirclement and a NO/NO_2 ratio of 0.6. The resulting NO_x total emissions within the IRVR are 3.7 ± 1.6 ton/h, 4.8 ± 2.6 ton/h and 4.8 ± 2.4 ton/h for the three campaigns. The NO_x vehicle emissions of the central

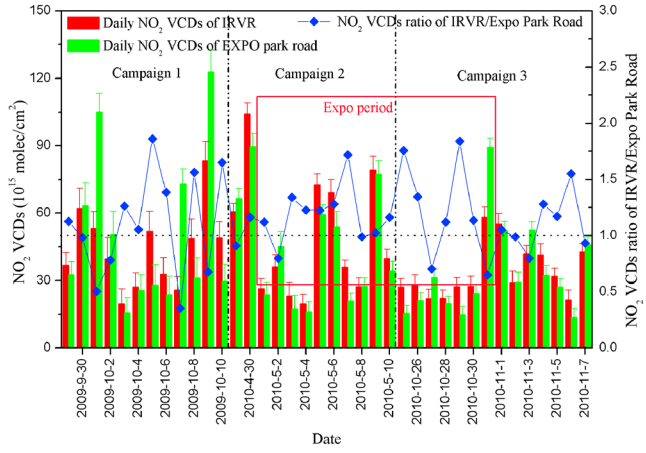

Figure 11. The comparison between daily averaged NO_2 VCDs of EXPO park road and IRVR during the three campaigns.

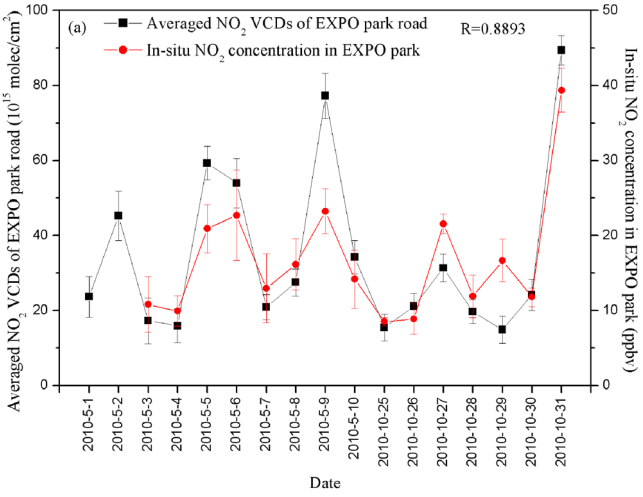

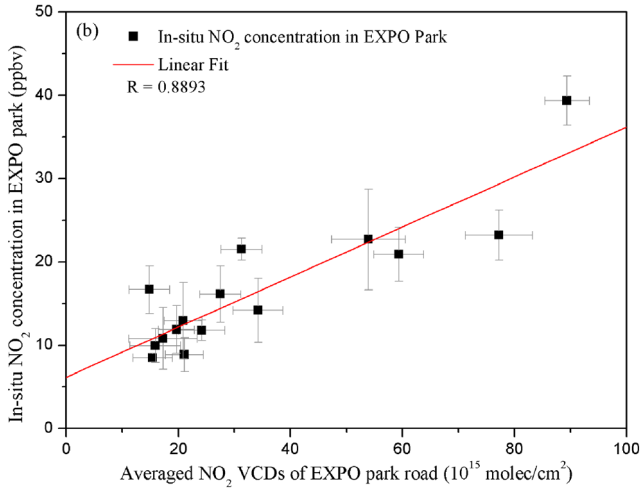

Figure 12. The comparison between daily averaged NO_2 VCDs of EXPO park road and corresponding averaged in situ NO_2 concentrations measured in EXPO park during the EXPO period.

urban area were derived from the total NO_x emissions based on a central urban area traffic emission share of 80.9% [*Fu*, 2009] resulting in hourly NO_x vehicle emissions of 3.0 ± 1.3 ton/h for 2009 and 3.9 ± 1.9 ton/h for 2010. Table 2 summarizes all the results of the mobile DOAS measurement for the NO_2 emissions, for the calculated NO_x vehicle emissions of both the central urban area as well as the whole city. In addition, this table shows the emission inventories of 2006 and the vehicle populations for 2006 and 2009.

[44] The diurnal NO_x cycle usually displays a typical double peak, representing heavy traffic in the morning and evening rush hours, indicating that NO_x emissions are mostly of vehicular origin [*Ran et al.*, 2009]. Considering that NO_x emissions were determined only around noontime, we make a reference to the diurnal vehicle emissions profile of Shanghai published by *Wang et al.* [2008]. They report that the emission peaks in the rush hour periods contributed about 54% to 56% of the total diurnal vehicle emissions in Shanghai, and the emission during the noon time (11:00 to 13:00) contributed about 9.3% of the total diurnal vehicle emissions. We have used these contribution shares to estimate daily emissions and annual emissions

Table 2. Hourly NO_2 and NO_x Total Emissions From the Central Urban Area Within the IRVR in Shanghai for 2009 and 2010 and Annual NO_x Vehicle Emissions Within IRVR and the Whole City, As Well As the NO_x Emission Inventories in 2006 (10^4 ton/yr)

Year	Vehicle Population ($\times 10^4$)	Emission Within IRVR (ton/h)		NO_x Vehicle Emission[c] (10^4 ton/yr)	
		Total NO_2[a]	Total NO_x[b]	IRVR	Whole City
2006[d]	238.13	–	–	1.46	8.44
2009	285.00	2.1 ± 0.8	3.8 ± 1.5	2.4 ± 1.0	13.5 ± 5.4
2010	309.70	2.7 ± 1.4	4.9 ± 2.6	3.1 ± 1.6	17.1 ± 9.0

[a]Calculated from the field measurements.
[b]Deduced from the field measurements according to two corrections for typical ratio of NO/NO_2 and NO_x lifetime.
[c]Estimated based on traffic emission share of NO_x in central urban area, and the same traffic emission share of central urban area to whole city in 2006.
[d]Quoted from the emission inventory of Shanghai in 2006.

from the hourly emissions quantified by the mobile DOAS method.

[45] The resulting annual vehicle NO_x emissions for the central urban area are $(2.3 \pm 1.0) \times 10^4$ ton in 2009 and $(3.0 \pm 1.5) \times 10^4$ ton in 2010. Additionally, the vehicle NO_x emissions of the whole city were determined to $(13.4 \pm 5.9) \times 10^4$ ton in 2009 and $(17.6 \pm 8.4) \times 10^4$ ton in 2010 by using the central urban area traffic volume share to that of the whole city of 2006 reported by *Fu* [2009]. Compared to a total NO_x emission of 1.8×10^4 ton and a vehicle NO_x emission of 1.46×10^4 ton within the IRVR reported in a emission inventory of 2006 [*Fu*, 2009], the NO_x emissions rate derived in this study show an increase by 1.6 times and 2.1 times from 2006 to 2009 and 2010, respectively. The elevated NO_x emissions appeared are possible a result of an increased vehicle population and traffic density.

[46] For the error of NO_x flux for each finite path element, another two more items, the NO/NO_2 ratio (R) and the NO_x lifetime correction (c_t), are also involved in:

$$\frac{\Delta F_{iNO_x}}{F_{iNO_x}} = \sqrt{\left(\frac{\Delta R}{R+1}\right)_i^2 + \left(\frac{\Delta c_t}{c_t}\right)_i^2 + \left(\frac{\Delta AMF}{AMF}\right)_i^2 + \left(\frac{\Delta \vec{W}}{\vec{W}}\right)_i^2 + \left(\frac{\Delta DSCD}{DSCD}\right)_i^2}. \quad (11)$$

[47] Together with the error of NO/NO_2 ratio evaluated to be 20–30% and NO_x lifetime to be about 10%, the relative error of the NO_x flux measurement was estimated to be about 55%. The standard deviation of the estimated NO_x emission rate is due to actual variations in the observed emissions from the IRVR, as well as the uncertainty in several items mentioned above.

4. Conclusion

[48] In this study we used the mobile DOAS technique to derive the NO_2 emission rates from the central urban area encircled by IRVR in Shanghai, China. The daily average NO_2 VCDs from mobile DOAS measurements have compared to those from GOME-2 observations. Moreover, the spatial distributions of NO_2 along the encircled route have been derived. Under the impacts of high traffic volume and the bad operating condition of vehicles, the main peak NO_2 columns along the route usually occurred at traffic congested junctions of the IRVR with other roads. The NO_2 spatial distribution is strongly dependent on wind conditions, i.e., the downwind NO_2 VCDs are generally higher than the upwind during the three campaigns. We found that the NO_2 VCDs decrease with increasing wind speed, especial when the wind speeds is higher than 4 m/s.

[49] The total NO_2 emissions emitted from the central urban area have been estimated to be 2.1 ± 0.9 ton/h, 2.8 ± 1.4 ton/h, and 2.7 ± 1.4 ton/h for the three campaigns. Using a typical NO/NO_2 ratio of 0.6, a NO_x lifetime of 5 h and the traffic emission shares for the central urban area of Shanghai, the estimated NO_x vehicle emissions within IRVR amount to 3.0 ± 1.3 ton/h for 2009 and 3.9 ± 1.9 ton/h for 2010, respectively. Accounting for the diurnal vehicle emissions profile of Shanghai, the annual vehicle NO_x emissions for the central urban area has been estimated to be $(2.3 \pm 1.0) \times 10^4$ ton in 2009 and $(3.0 \pm 1.5) \times 10^4$ ton in 2010, and for the entire city to be $(13.4 \pm 5.9) \times 10^4$ ton in 2009 and $(17.6 \pm 8.4) \times 10^4$ ton in 2010. These results show an increasing trend of vehicle NO_x emission from central urban area in Shanghai, and are consistent with the increases of vehicle population.

[50] Comparing with the bottom-up emission inventories that a time lag of generally 3–4 years and are prone to uncertainties due to errors in amount and strength of individual pollutant sources, mobile DOAS measurements are a fast and feasible method to estimate pollutant emissions from a point source or even a large area source like an industrial zone or an entire city. Furthermore this method is capable of verifying the accuracy of emission inventories and contributing to renewing existing estimates for pollutant emission data. However, uncertainties in the emission estimates by the mobile DOAS method for the IRVR area are introduced by wind field variations, unknown NO_x chemical transformation, and atmospheric scattering complicated by the presence of clouds and aerosols. As a result, we estimate the systematic deviation of the vehicle NO_x emissions is 55%.

[51] To reduce the uncertainties in the estimated emissions, future mobile DOAS measurements should be conducted preferably during clear sky days and stable solar light and wind conditions. Ideal measurement conditions are characterized by no or smaller increase of the NO_2 amount within IRVR, moderate wind speed, and relatively larger difference between upwind and down NO_2 VCDs. The accuracy of the determination of the NO_2 VCDs should be improved using a

more accurate AMF calculation. More perfect wind data would be helpful to determine the emissions, e.g., using the measured vertical wind profile relevant for the transported layer of the NO_2 or coupling it with concurrent meso-scale transport models to improve the emission analysis. Besides, more detailed data on chemical concentrations (e.g., O_3, OH radicals) would be useful to quantify the chemical transformation correction factors. Finally, mobile DOAS measurements could be applied to cover temporal variations (from diurnal to seasonal variations) for various spatial scales (from the central urban area encircled by IRVR to the whole Shanghai city encircled by the outer ring road).

[52] **Acknowledgments.** This work was supported by the National Natural Science Foundation of China under grants 40975076 and National High-tech R&D Program ("863" Program, 2009AA063006, 2006AA06Z417). We also thank the support of China Meteorological Administration (grant GYHY201106045–8) and Shanghai Environmental Protection Bureau. We would like to thank the Remote Sensing Technology Institute of German Aerospace Center (DLR-IMF) for supplying the GOME-2 tropospheric NO_2 vertical column density data. The WinDOAS spectral analysis software was developed by Caroline Fayt and Michel van Roozendael in IASB/BIRA Uccle, Belgium. Helpful technical discussions with colleagues from the GIS group in our department at Fudan University are acknowledged. Great thanks are given to Manfred Gottwald at DLR-IMF for improvements in reviewing the manuscript.

References

Atkinson, R. (2000), Atmospheric chemistry of VOCs and NO_x, *Atmos. Environ.*, *34*, 2063–2101, doi:10.1016/S1352-2310(99)00460-4.

Bobrowski, N., and U. Platt (2007), SO_2/BrO ratios studied in five volcanic plumes, *J. Volcanol. Geotherm. Res.*, *166*, 147–160, doi:10.1016/j.jvolgeores.2007.07.003.

Burrows, J. P., A. Dehn, B. Deters, S. Himmelmann, A. Richter, S. Voigt, and J. Orphal (1998), Atmospheric remote-sensing reference data from GOME: Part 1. Temperature-dependent absorption cross sections of NO_2 in the 231–794 nm range, *J. Quant. Spectrosc. Radiat. Transfer*, *60*, 1025–1031, doi:10.1016/S0022-4073(97)00197-0.

Burrows, J. P., A. Richter, A. Dehn, B. Deters, S. Himmelmann, S. Voigt, and J. Orphal (1999), Atmospheric remote-sensing reference data from GOME: Part 2. Temperature-dependent absorption cross sections of O_3 in the 231–794 nm range, *J. Quant. Spectrosc. Radiat. Transfer*, *61*, 509–517, doi:10.1016/S0022-4073(98)00037-5.

Chan, C. K., and X. H. Yao (2008), Air pollution in mega cities in China, *Atmos. Environ.*, *42*, 1–42, doi:10.1016/j.atmosenv.2007.09.003.

Chen, D., B. Zhou, S. Beirle, L. M. Chen, and T. Wagner (2009), Tropospheric NO_2 column densities deduced from zenith-sky DOAS measurements in Shanghai, China, and their application to satellite validation, *Atmos. Chem. Phys.*, *9*, 3641–3662, doi:10.5194/acp-9-3641-2009.

Fayt, C., and M. Van Roozendael (2001), *WinDOAS 2.1 Software User Manual*, IASB-BIRA, Belgium.

Fraser, A., C. Adams, J. R. Drummond, F. Goutail, G. Manney, and K. Strong (2009), The Polar Environment Atmospheric Research Laboratory UV–visible Ground-Based Spectrometer: First measurements of O_3, NO_2, BrO, and OClO columns, *J. Quant. Spectrosc. Radiat. Transfer*, *110*, 986–1004, doi:10.1016/j.jqsrt.2009.02.034.

Fu, Q. Y. (2009), Emission inventory and the formation mechanism of high pollution of fine particulate matters in Shanghai, PhD thesis, Dep. of Environ. Sci. and Eng., Fudan Univ., Shanghai, China.

Geng, F. H., X. X. Tie, J. M. Xu, G. Q. Zhou, L. Peng, W. Gao, X. Tang, and C. S. Zhao (2008), Characterizations of ozone, NO_x, and VOCs measured in Shanghai, China, *Atmos. Environ.*, *42*, 6873–6883, doi:10.1016/j.atmosenv.2008.05.045.

Giovanelli, G., E. Palazzi, A. Petritoli, D. Bortoli, I. Kostadinov, F. Margelli, S. Pagnutti, M. Premuda, F. Ravegnani, and G. Trivellone (2006), Perspectives of 2D and 3D mapping of atmospheric pollutants over urban areas by means of airborne DOAS spectrometers, *Ann. Geophys.*, *49*, 133–142.

Greenblatt, G. D., J. J. Orlando, J. B. Burkholder, and A. R. Ravishankara (1990), Absorption measurements of oxygen between 330 and 1140 nm, *J. Geophys. Res.*, *95*(D11), 18,577–18,582, doi:10.1029/JD095iD11p18577.

Ibrahim, O., R. Shaiganfar, R. Sinreich, T. Stein, U. Platt, and T. Wagner (2010), Car MAX-DOAS measurements around entire cities: Quantification of NO_x emissions from the cities of Mannheim and Ludwigshafen (Germany), *Atmos. Meas. Tech.*, *3*, 709–721, doi:10.5194/amt-3-709-2010.

Institute of Remote Sensing (2007), User's guide for the software package SCIATRAN (Radiative Transfer Model and Retrieval Algorithm), version 2.2, report, Univ. of Bremen, Bremen, Germany.

Johansson, M., B. Galle, T. Yu, L. Tang, D. Chen, H. Li, J. X. Li, and Y. Zhang (2008), Quantification of total emission of air pollutants from Beijing using mobile mini-DOAS, *Atmos. Environ.*, *42*, 6926–6933, doi:10.1016/j.atmosenv.2008.05.025.

Johansson, M., C. Rivera, B. de Foy, W. Lei, J. Song, Y. Zhang, B. Galle, and L. Molina (2009), Mobile mini-DOAS measurement of the outflow of NO_2 and HCHO from Mexico City, *Atmos. Chem. Phys.*, *9*, 5647–5653, doi:10.5194/acp-9-5647-2009.

Leitão, J., A. Richter, M. Vrekoussis, A. Kokhanovsky, Q. J. Zhang, M. Beekmann, and J. P. Burrows (2010), On the improvement of NO_2 satellite retrievals-aerosol impact on the airmass factors, *Atmos. Meas. Tech.*, *3*, 475–493, doi:10.5194/amt-3-475-2010.

Lin, J. T., M. B. McElroy, and K. F. Boersma (2010), Constraint of anthropogenic NO_x emissions in China from different sectors: A new methodology using multiple satellite retrievals, *Atmos. Chem. Phys.*, *10*, 63–78, doi:10.5194/acp-10-63-2010.

Martin, R. V. (2008), Satellite remote sensing of surface air quality, *Atmos. Environ.*, *42*, 7823–7843, doi:10.1016/j.atmosenv.2008.07.018.

McGonigle, A. J. S., C. L. Thomson, V. I. Tsanev, and C. Oppenheimer (2004), A simple technique for measuring power station SO_2 and NO_2 emissions, *Atmos. Environ.*, *38*, 21–25, doi:10.1016/j.atmosenv.2003.09.048.

McLinden, C. A., J. C. McConnell, E. Griffioen, and C. T. McElroy (2002), A vector radiative transfer model for the Odin/OSIRIS project, *Can. J. Phys.*, *80*, 375–393, doi:10.1139/p01-156.

Munro, R., M. Eisinger, C. Anderson, J. Callies, E. Corpaccioli, R. Lang, A. Lefebvre, Y. Livschitz, and A. Perez Albinana (2006), GOME-2 on METOP: From in-orbit verification to routine operations, paper presented at Meteorological Satellite Conference, EUMETSAT, Helsinki.

Pan, L., H. Z. Che, F. H. Geng, X. G. Xia, Y. Q. Wang, C. Z. Chi, M. Chen, W. Gao, and J. P. Guo (2010), Aerosol optical properties based on ground measurements over Chinese Yangtze Delta Region, *Atmos. Environ.*, *44*, 2587–2596, doi:10.1016/j.atmosenv.2010.04.013.

Petritoli, A., G. Giovanelli, I. Kostadinov, F. Ravegnani, D. Bortoli, P. Bonasoni, F. Evangelisti, U. Bonafe, and F. Calzolari (2002), Tropospheric and stratospheric NO_2 amount deduced by slant column measurements at Mt. Cimone Station, *Adv. Space Res.*, *29*, 1691–1695, doi:10.1016/S0273-1177(02)00121-7.

Petritoli, A., P. Bonasoni, G. Giovanelli, F. Ravegnani, I. Kostadinov, D. Bortoli, A. Weiss, D. Schaub, A. Richter, and F. Fortezza (2004), First comparison between ground-based and satellite-borne measurements of tropospheric nitrogen dioxide in the Po basin, *J. Geophys. Res.*, *109*, D15307, doi:10.1029/2004JD004547.

Platt, U., and J. Stutz (2008), *Differential Optical Absorption Spectroscopy: Principles and Applications*, Springer, Berlin.

Ran, L., C. S. Zhao, F. H. Geng, X. X. Tie, X. Tang, L. Peng, G. Q. Zhou, Q. Yu, J. M. Xu, and A. Guenther (2009), Ozone photochemical production in urban Shanghai, China: Analysis based on ground level observations, *J. Geophys. Res.*, *114*, D15301, doi:10.1029/2008JD010752.

Rivera, C., G. Sosa, W. Wohrnschimmel, B. de Foy, M. Johansson, and B. Galle (2009), Tula industrial complex (Mexico) emissions of SO_2 and NO_2 during the MCMA 2006 field campaign using a mobile mini-DOAS system, *Atmos. Chem. Phys.*, *9*, 6351–6361, doi:10.5194/acp-9-6351-2009.

Rivera, C., J. Mellqvist, J. Samuelsson, B. Lefer, S. Alvarez, and M. R. Patel (2010), Quantification of NO_2 and SO_2 emissions from Houston Ship Channel and Texas City industrial areas during the 2006 Texas Air Quality Study, *J. Geophys. Res.*, *115*, D08301, doi:10.1029/2009JD012675.

Rothman, L. S., et al. (1998), The HITRAN molecular spectroscopic database and HAWKS (HITRAN atmospheric workstation): 1996 edition, *J. Quant. Spectrosc. Radiat. Transfer*, *60*, 665–710, doi:10.1016/S0022-4073(98)00078-8.

Shaiganfar, R., S. Beirle, M. Sharma, A. Chauhan, R. P. Singh, and T. Wagner (2011), Estimation of NO_x emissions from Delhi using car MAX-DOAS observations and comparison with OMI satellite data, *Atmos. Chem. Phys.*, *11*, 10,871–10,887, doi:10.5194/acp-11-10871-2011.

Shanghai Municipal Statistics Bureau (2001–2010), *Shanghai Statistical Yearbook 2001–2010*, China Stat., Beijing, China.

United Nations Environment Programme (UNEP) (2009), Vehicle emission control, in *UNEP Environmental Assessment EXPO 2010 Shanghai, China, DCP/1209/NA*, pp. 49–50, UNEP, Nairobi.

Valks, P., D. Loyola, N. Hao, M. Rix, and S. Slijkhuis (2011a), Algorithm theoretical basis document for GOME-2 total column products of ozone, NO_2, tropospheric NO_2, BrO, SO_2, H_2O, HCHO, OClO and cloud properties (GDP 4.4 for O3M-SAF OTO and NTO), *DLR/GOME-2/ATBD/01*, DLR, Oberpfaffenhofen, Germany. [Available at http://wdc.dlr.de/sensors/gome2/DLR_GOME-2_ATBD_2A.pdf.]

Valks, P., G. Pinardi, A. Richter, J.-C. Lambert, N. Hao, D. Loyola, M. Van Roozendael, and S. Emmadi (2011b), Operational total and tropospheric NO_2 column retrieval for GOME-2, *Atmos. Meas. Tech.*, *4*, 1491–1514, doi:10.5194/amt-4-1491-2011.

Wagner, T., B. Dix, C. V. Friedeburg, U. Frieß, S. Sanghavi, R. Sinreich, and U. Platt (2004), MAX-DOAS O_4 measurements: A new technique to derive information on atmospheric aerosols: Principles and information content, *J. Geophys. Res.*, *109*, D22205, doi:10.1029/2004JD004904.

Wang, H. K., C. H. Chen, C. Huang, and L. X. Fu (2008), On-road vehicle emission inventory and its uncertainty analysis for Shanghai, China, *Sci. Total Environ.*, *398*, 60–67, doi:10.1016/j.scitotenv.2008.01.038.

Wang, H. K., L. X. Fu, Y. Zhou, X. Du, and W. H. Ge (2010), Trends in vehicular emissions in China's mega cities from 1995 to 2005, *Environ. Pollut.*, *158*, 394–400, doi:10.1016/j.envpol.2009.09.002.

Wang, S. S., B. Zhou, Q. Ye, and F. Qi (2009), Application of vehicle-borne passive differential optical absorption spectroscopy for urban traffic air pollution monitoring, *Acta Opt. Sin.*, *29*, 2645–2649, doi:10.3788/AOS20092910.2645.

Yang, Y. J., J. G. Tan, Y. F. Zheng, and S. H. Cheng (2006), Study on the atmospheric stabilities and the thickness of atmospheric mixed layer during recent 15 years in Shanghai, *Sci. Meteorol. Sin.*, *26*, 536–541.